Available online at www.sciencedirect.com
ScienceDirect
Journal of Molecular Catalysis A: Chemical 281 (2008) 99–106
JOURNAL OF MOLECULAR CATALYSIS A: CHEMICAL
www.elsevier.com/locate/molcata

Photocatalytic reaction of acetaldehyde over $SrTiO_3$ nanoparticles

Chih-Ang Chang [a], Brian Ray [a], Dilip K. Paul [a,*], Dmytro Demydov [b], Kenneth J. Klabunde [b]

[a] *Department of Chemistry, Pittsburg State University, Pittsburg, KS 66762, United States*
[b] *Department of Chemistry, Kansas State University, Manhattan, KS 66506, United States*

Available online 19 August 2007

Abstract

The photooxidation of acetaldehyde on $SrTiO_3$ has been studied using UV–vis irradiation in the range of 2.1–5.0 eV. It has been found that a large fraction of acetaldehyde undergoes aldol condensation during dark oxidation forming crotonaldehyde. However, in presence of UV light, the formation of CO_2 and other partially oxidized species was observed. The infrared assignment of surface species was used to explore the photochemical reaction.

Keywords: Acetaldehyde; FT-IR; $SrTiO_3$; Nanoparticles; Photooxidation; Photocatalytic reaction

1. Introduction

Titanium dioxide (TiO_2) and other oxides with similar semiconductor properties such as $SrTiO_3$ (perovskite structure with band gap ~3.2 eV) have attracted considerable attention because of their unique properties for photochemical oxidation of organic molecules [1–3]. However, the nature of acid–base sites is expected to be different because of the presence of Sr which is more ionic in $SrTiO_3$ than in SrO, and Ti is more covalent in $SrTiO_3$ than in TiO_2 [3]. This results in an increase in the covalent properties or weakening of the acidity of Ti ion. Thus, the nature of bonding of an adsorbate may be significantly different from TiO_2, which may lead to different photochemical reactivities. After the discovery of photo-induced water-splitting at titanium dioxide electrodes [4], the phenomena have been applied to TiO_2 mediated heterogeneous photocatalysis. Because electrons and holes photogenerated in the semiconductor photocatalysts have strong reduction and oxidation potential, they can drive a variety of reactions [5–9].

In addition, adsorption and reaction of oxygenated hydrocarbons on metal oxide surfaces are of much interest from both fundamental and practical perspectives. The chemistry of oxygenated hydrocarbons on metal oxide surfaces is rich and complex, involving a variety of catalytic processes such as selective oxidation, reduction, and condensation. The reactivity largely depends on the characteristics of the oxide catalysts defined by their surface structures, acid–base properties, and surface defects.

Although there have been a few studies of acetaldehyde adsorption, thermal oxidation, and photocatalytic oxidation over TiO_2, there is no report on adsorption and photocatalytic reaction of acetaldehyde over high surface area $SrTiO_3$. In this study, we introduce an *in situ* approach to study the chemistry of acetaldehyde over a $SrTiO_3$ surface during adsorption and photochemical reaction, namely transmission FT-IR spectroscopy [10,11]. This technique has been able to provide invaluable and complementary structural and dynamic information due to its high resolution and quantitative capabilities. In particular, IR is well suited to follow the formation and evolution of surface-bound species on the catalysts. $SrTiO_3$ nanoparticles used in this study were prepared by conventional sol–gel techniques as described below.

2. Experimental

2.1. Synthesis and characterization of $SrTiO_3$

The synthesis of aerogel prepared [12–14] nanostructured strontium titanate (AP-$SrTiO_3$) consists of several steps: the

* Corresponding author. Tel.: +1 620 235 4872; fax: +1 620 235 4003.
E-mail address: dpaul@pittstate.edu (D.K. Paul).

1381-1169/$ – see front matter © 2007 Elsevier B.V. All rights reserved.
doi:10.1016/j.molcata.2007.08.014

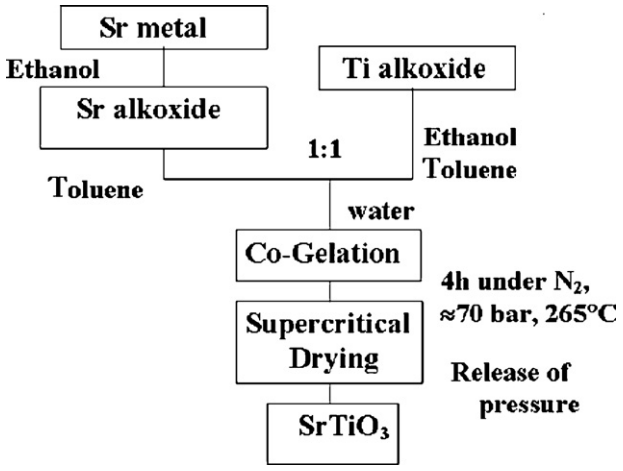

Fig. 1. Schematic of Aerogel procedure for $SrTiO_3$ synthesis.

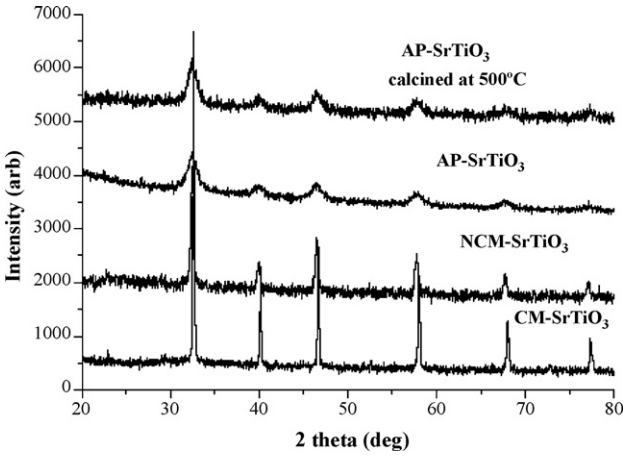

Fig. 2. Powder XRD patterns of commercial and synthesized $SrTiO_3$ (CM, commercial; NCM, nanosized commercial; AP, aerogel prepared samples).

preparation of alkoxide mixtures in an alcohol–toluene solvent, hydrolysis, co-gelation of alkoxides, and solvent removal by a supercritical drying step as shown in Fig. 1.

The process involves the production of a three-dimensional polymeric gel network from metal alkoxides followed by solvent removal using supercritical drying, which prevents the collapse of the network and preserves the unique properties of the product, such as high porosity, small crystallite sizes, and large surface area.

Here a mixture of alcohol and toluene solvent is essential for obtaining intimately mixed metal oxides with high surface areas and small crystallite sizes. AP-$SrTiO_3$ was prepared in an ethanol mixture with toluene in a toluene-to-alcohol volume-ratio of 1.5. The mixture of metal alkoxides and alcohol–toluene was hydrolyzed with water by a slow, dropwise addition, to transform it into a gel. Supercritical conditions were achieved by heating in an autoclave under a nitrogen atmosphere. The solvent vapors were removed by quick venting of the solvent, and the residual solvent in the prepared aerogel powders was removed by calcination in air at 773 K.

The structural and textural properties were investigated by powder X-ray diffraction (Fig. 2) and by BET analysis using nitrogen adsorption at 77 K (Table 1).

The aerogel prepared $SrTiO_3$ samples have smaller crystallite sizes and significantly higher surface areas in comparison with available commercial samples (from Sigma–Aldrich or Alfa-Aesar).

The crystallite morphology of strontium titanate samples estimated using two complimentary techniques of TEM (Fig. 3) and powder XRD (Fig. 2). Transmission electron micrographs confirmed the crystallite sizes of samples derived from XRD peaks using the Debye–Scherrer equation. Strontium titanate prepared by the aerogel method has a crystallite size of 8 ± 2 nm in comparison with 145 nm of the commercial CM-$SrTiO_3$, and 25 nm of nanosized commercial NCM-$SrTiO_3$. In aerogel samples, crystallite sizes after calcination were slightly larger in comparison with crystallites of freshly prepared aerogels. All crystallites had uniform spherical shapes with a size distribution near 8 ± 2 nm for synthesized AP-$SrTiO_3$ and near 10 ± 2 nm for calcined AP-$SrTiO_3$ at 500 °C in air. The shapes of aerogel crystallites had a defined spherical form and sizes are relatively monodispersed, while commercial CM-$SrTiO_3$ samples have non-uniform shapes and polydispersed sizes.

2.2. Infrared study

The powdered samples were hydraulically pressed at 12,000 lbs/in.^{2} onto a tungsten mesh [15] (0.0508 mm thick, with 0.22 mm^2 holes) as a circular spot of 7 mm in diameter, typically weighing 1–1.5 mg (1.3–1.9 mg/cm^2) [15]. The transparency of the grid to the IR beam is about 80%, so that infrared radiation can pass through the sample efficiently. The grid is supported in the center of the stainless steel cell [16] by nickel clamps along the grid edges. A chromel/constantan thermocouple spot-welded to the top center region of the grid, is used for temperature control. Electrical heating and cooling with liquid nitrogen and a power supply/temperature programmer permit the temperature of the grid to be maintained to about ±2 K within the range 100–1500 K. The IR cell is connected through a gas port to a high vacuum system, equipped with a quadrupole mass spectrometer. The base pressure of the system is kept below 10^{-8} Torr by a Pfeiffer Vacuum 60 l/s turbomolecular pump backed by

Table 1
Textural properties of different $SrTiO_3$ samples

$SrTiO_3$ sample	Average crystallite sizes (nm)	Surface area (m^2 g^{-1})
Commercial (CM-$SrTiO_3$)	145	1
Nanosized commercial (NCM-$SrTiO_3$)	25	17
Aerogel (AP-$SrTiO_3$) after synthesis	8	159
Aerogel (AP-$SrTiO_3$) after calcination in air at 500 °C	10	93

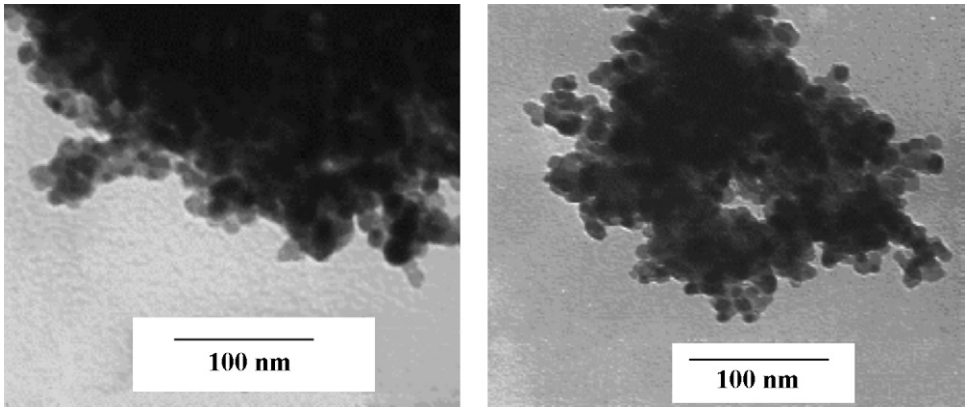

Fig. 3. TEM graphs of AP-$SrTiO_3$ after synthesis (left) and after calcination in air at 500 °C (right).

an oil-free diaphragm pump. The pressure was measured by a capacitance manometer (Baratron, 116A, MKS, range 10^{-3} to 10^3 Torr) or by the ion current drawn by the ion pump. The cell windows were KBr single crystals mounted on concentric Viton O-rings which are differentially pumped to prevent leaks.

The IR cell is mounted on a computer-controlled translation system (Newport Corporation), capable of moving the cell to ±1 μm accuracy in the horizontal and vertical directions. Thus, it is possible to study two samples, i.e. $SrTO_3$ and TiO_2 at the middle and the bottom positions on the same grid for comparison of their spectroscopic and adsorptive properties under identical conditions of temperature and gas exposure. The upper one-third positions on the grid were empty and were used for the background absorbance measurements in the same experiments.

The light source was a 100 W Xenon Arc Lamp (Photon Technology International) which was focused onto the sample through a quartz window. The light was filtered with a water filter to remove IR radiation and was focused onto the sample through a sapphire window. The intensity of the UV radiation on the sample was 70 mW/cm^2 in the range of 2.1–5 eV.

Infrared spectra were obtained with a dry CO_2-free air purged Mattson Research Series I FTIR spectrometer equipped with a narrow band HgCdTe detector operating at 77 K. The sample and background spectra shown here were recorded in the ratio mode with a resolution of 4 cm^{-1} using 300 scans. Acetaldehyde (99%) and crotonaldehyde (99%) used for this work were obtained from Aldrich. These liquids were stored in glass bulbs and purified by five freeze-pump-thaw cycles using the high vacuum system. The oxygen used was obtained from Matheson and was 99.999% pure.

The oxide samples were heated in vacuum at 473 K for ~10 h and then the temperature was gradually to 773 K for calcination with 20.0 Torr oxygen followed by evacuation. The evacuated sample was then heated at 873 K for 30 min before cooling. This procedure allows the removal of traces of residual organic species which could come from remnant alkoxy groups retained by the oxide nanoparticles after the preparation procedure. Before exposure to adsorbates, the samples were cooled in vacuum to 233 K. Adsorption of acetaldehyde, crotonaldehyde, and FTIR measurements was carried out at different temperatures beginning at 233 K. For a typical experiment, about 0.1 Torr acetaldehyde was exposed to $SrTiO_3$ for an hour at 233 K followed by evacuation for 15 min. However, for the dark and photooxidation, sample has been warmed up to 258 and 273 K, respectively.

3. Results and discussion

3.1. Acetaldehyde adsorption over $SrTiO_3$ at 233 K: evidence of irreversible H-bonding

Fig. 4(a) shows the background spectrum of $SrTiO_3$ taken at 233 K upon calcination followed by thermal treatment at 923 K. Here the OH region shows a prominent infrared feature at 3689 cm^{-1} which can be assigned mainly to the ν(OH) mode for isolated hydroxyl groups bound to Ti atoms consistent with the assignment of earlier work involving TiO_2 based binary oxides [17,18].

Although a minute contribution to the intensity of 3689 cm^{-1} band may also arise from the OH stretching modes for $Sr(OH)_2$ species, which usually appears at 3698 cm^{-1} [17,18]. In a recent TiO_2 study, Panayotov and Yates identified a small feature at ~3700 cm^{-1}, assigned to isolated Ti–OH groups. This 11 cm^{-1} red-shift may be due to electron donating effect of the alkaline earth metal ion, Sr^{n+}. And the weak low frequency band at 3403 cm^{-1} can be assigned to either Ti–OH perturbed by nearby Sr atoms or to Sr–OH groups [18].

The presence of the strong broad feature at 1435 cm^{-1} can be assigned to ν_{asym}(OCO) groups for CO_3^{2-} groups formed from residual organic precursor/solvent during the calcination of nanoparticles. All studies on carbonate surface species including a recent work on iron oxide studied by IR spectroscopy showed that peak for CO_3^{2-} appears at 1490–1450 cm^{-1} [19].

All other spectra shown in Fig. 4 are obtained by subtraction of the background spectrum (a). Upon exposure of 0.1 Torr acetaldehyde for an hour at 233 K, the evolution of ν(CH) and δ(CH) modes along with concomitant depletion of ν(OH) absorbance are clearly observed as shown in spectrum (b).

The dominant spectral features in the ν(CH) region at 2973 and 2928 cm^{-1} can be assigned to $\nu_a(CH_3)$ and $\nu_s(CH_3)$ of acetaldehyde adsorbed onto the surface mainly through H-bonding, whereas the mode at 2867 cm^{-1} is due to the overtone

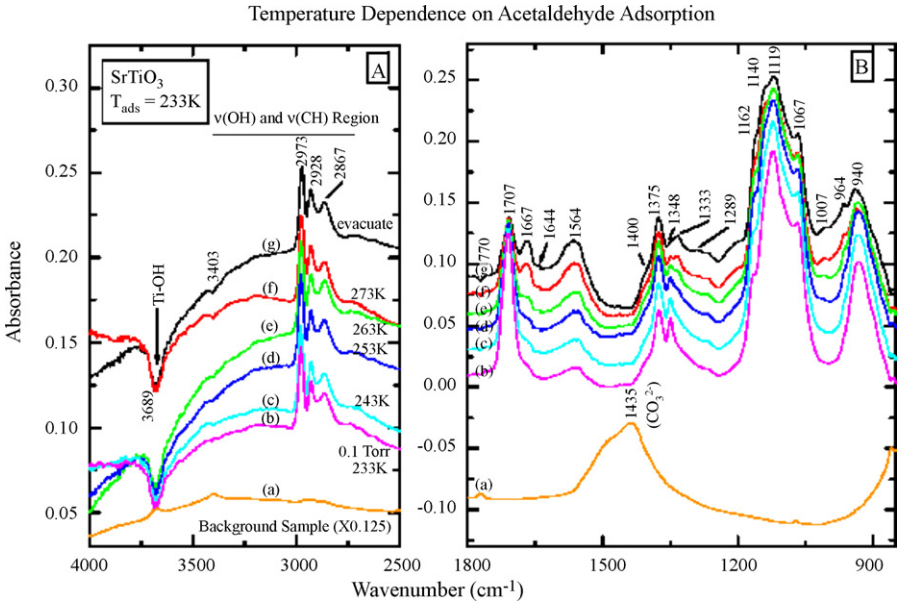

Fig. 4. (A and B) Infrared spectra of 0.1 Torr acetaldehyde (CH_3CHO) adsorbed on $SrTiO_3$ at 233 K followed by warming up (spectra (b)–(f)) and evacuation (spectrum (g)) at 273 K. Spectra (b)–(f) are obtained by subtraction of background spectrum (a).

for δ(CH) mode. The depletion of isolated Ti–OH intensity at 3689 cm^{-1} with an increase in intensity of the band in the low frequency side (3550–3350 cm^{-1}) indicates the formation of H-bonds through oxygen of the carbonyl group [$TiOH\cdots O=C(H)CH_3$] [20–22]. Hydrogen bonding is generally characterized by (a) frequency shifts to lower frequency of the absorption bands due to ν(OH) stretching vibration and (b) broadening of the shifted OH band along with an increase in the absorbance. Upon evacuation for 15 min at 1×10^{-6} Torr, no apparent changes in spectral behavior were observed indicating the irreversibility of H-bonding. The configuration of irreversibly bound CH_3–CHO species is most likely that in which the partially negative charged oxygen moiety of acetaldehyde interacts with positively charged hydrogen moiety of the surface hydroxyl groups, leaving the methyl moiety largely unperturbed relative to its behavior in the gas phase. This configuration is most probable since gas phase of CH_3CHO possesses a substantial dipole moment of 2.7 Debye. The relatively minor frequency and intensity changes in the observed $\nu(CH_3)$ and $\delta(CH_3)$ vibrational modes are a consequence of the local mode character of the CH_3 groups [22].

A fraction of acetaldehyde may also be adsorbed through $>C=O\rightarrow Ti^{4+}$ and/or Ti^{3+} ions, which forms by thermal treatment of TiO_2 under evacuation [23]. The fingerprint region shows a variety of deformation modes in addition to the strong ν(C=O) mode at 1707 cm^{-1} which are as explained below. The infrared features at 1375 and 1348 cm^{-1} can be assigned to $\delta_a(CH_3)$ and $\delta_s(CH_3)$, respectively, whereas the strong signature at 1119 cm^{-1} indicates the ν(C–C) mode. The strong feature at 940 cm^{-1} may be assigned to $\rho(CH_3)$ and is consistent with other studies. The weak feature at 1564 cm^{-1} along with a shoulder at ~1420 cm^{-1} (on the high frequency side of 1375 cm^{-1}) is attributed to ν_{as}(OCO) and ν_s(OCO), respectively, for the bidentate acetate species [$\nu_{as}(OCO)-\nu_s(OCO)=144\ cm^{-1}$]. The formation of acetate species from acetaldehyde molecules was previously observed on several oxide species including TiO_2, ZnO, and CeO_2 [24–26].

3.2. *Warm-up effects of adsorbed acetaldehyde: evidence of aldol condensation and formation of an α,β-unsaturated aldehyde, 2-butenal (crotonaldehyde, CH_3–CH=CH–CHO)*

As the temperature was raised at an interval of 10 °C (Fig. 4B, b–e), the decrease in intensities of spectral bands of surface bound acetaldehyde at 1707—ν(C=O), 1348—δ(CH), 1119—ν(C–C) and 940—$\gamma_r(CH_3)$ cm^{-1} can clearly be noticed. In addition, the new infrared spectral features appeared at 1667(s), 1644(shoulder), 1333, 1162, 1067, and 964 cm^{-1}. This change is accompanied by a slight decrease in intensity of ν(O–H) mode at 3403 cm^{-1} along with an increase in intensity of an unresolved broad ν(O–H) feature ~3250 cm^{-1}, indicating the probable formation of new aldol surface species formed by condensation of two acetaldehyde molecules having a ν(C–O) mode at 1007 cm^{-1} and the ν(C–C) unresolved mode at 1140 cm^{-1}. In addition, the $\delta(CH)_{ald}$ mode of acetaldehyde at 1348 cm^{-1} decreased in intensity forming a new band at 1333 cm^{-1} which can be assigned to $\delta(CH)_{ald}$ for aldol. The hydrogen atom from α-carbon of the first molecular acetaldehyde is abstracted by the surface oxide ion forming an enolate which then attacks the second carbonyl group of the other acetaldehyde bonded through H-bond to the surface –OH group. This nucleophilic addition produces aldol which is a very common intermediate in homogeneous organic reactions. The aldol ultimately dehydrates on the surface forming crotonaldehyde (an α,β-unsaturated aldehyde) surface species. The dehydration is clearly be evidenced by a gradual decrease in intensity of the >C=O mode at 1707 cm^{-1} with sequential growth of 1667 cm^{-1} feature accompanied by a weak ν(C=C) mode at 1644 cm^{-1}. The infrared frequency and

Table 2
Vibrational frequency (cm^{-1}) and assignments of adsorbed species (acetaldehyde and related surface species) during of acetaldehyde over $SrTiO_3$

Assignment	Gas phase	Ar matrix	TiO_2 anatase	$SrTiO_3$	Crotonaldehyde/$SrTiO_3$	Crotonaldehyde/Pt(1 1 1)
$\nu_{as}(CH_3)$	3014	3022	2969	2973	2969	
$\nu_s(CH_3)$	2968	2921	2914/2846	2928/2867	2919/2860	
$\nu(CH_{ald})$	2716	2736	2759	2755	2738	2750
$\nu(C{=}O)$	1743	1729	1718	1707	1667	1694
$\nu(C{=}C)$					1644	1644
$\delta_{as}(CH_3)$	1433	1427		1400	1455	1447
$\delta_s(CH_3)$	1395	1399	1355	1375	1394/1371	1397/1376
$\delta(CH)$	1352	1349		1348	1311	1300
$\nu(C–C)$	1114	1111		1119	1158	1158
$\nu(C–CH_3)$					1105	1083
$\gamma_r(CH_3)$	920/867	873		940	964	977
$\gamma(CH_3)$	764					

vibrational assignments of surface species for crotonaldehyde conversion during warm-up experiments is given in Table 2. The last column of the table correspond to the observation of crotonaldehyde condensation on Pt(1 1 1) [27] surface at 90 K and the data are consistent with infrared features seen for these studies. Several studies involving acetaldehyde both on single crystal and polycrystalline TiO_2 surfaces also noticed the aldol condensation reaction forming crotonaldehyde during temperature programmed desorption reactions [28–30].

3.3. Dark oxidation: influence of oxygen exposure over preadsorbed acetaldehyde at 258 K

Fig. 5 shows a series of subtracted (for clarity purposes) infrared spectra (for a duration of 85 min) obtained upon introduction of oxygen gas over preadsorbed acetaldehyde at 258 K. The reference spectrum used for subtraction purposes was Fig. 4A(g), which had been evacuated before introduction of 14.0 Torr O_2 in order to observe the effect of oxygen exposure in the dark (meaning without the irradiation of UV–vis light). It may be noted that at this temperature, below 1800 cm^{-1} region (Fig. 5B (a–f)) a number of bands (1668, ~1610, 1580, 1018, and 972 cm^{-1}) gained intensities as a function of time, while the other bands (1716, 1373, 1167, 1122, 1064, and 936 cm^{-1}) lost intensities within the same time period.

Here the decrease in intensity of 1716 cm^{-1} feature along with simultaneous decrease in intensities of ν(C–C) mode at 1122 cm^{-1} and $\nu(C–CH_3)$ mode at 1064 cm^{-1} indicate that both preadsorbed acetaldehyde and crotonaldehyde (formed during warm-up) are continually being oxidized forming carboxylate surface species showing a strong infrared feature ~1580 cm^{-1} and a medium intensity peak at 1424 cm^{-1} for ν_a(OCO) and ν_s(OCO) surface species.

However, there was no evidence found of formation of CO_2 for ν_a(OCO) in the 2300–2400 cm^{-1} region. In addition, there was no change in integrated absorbance for both ν_a(OCO) and

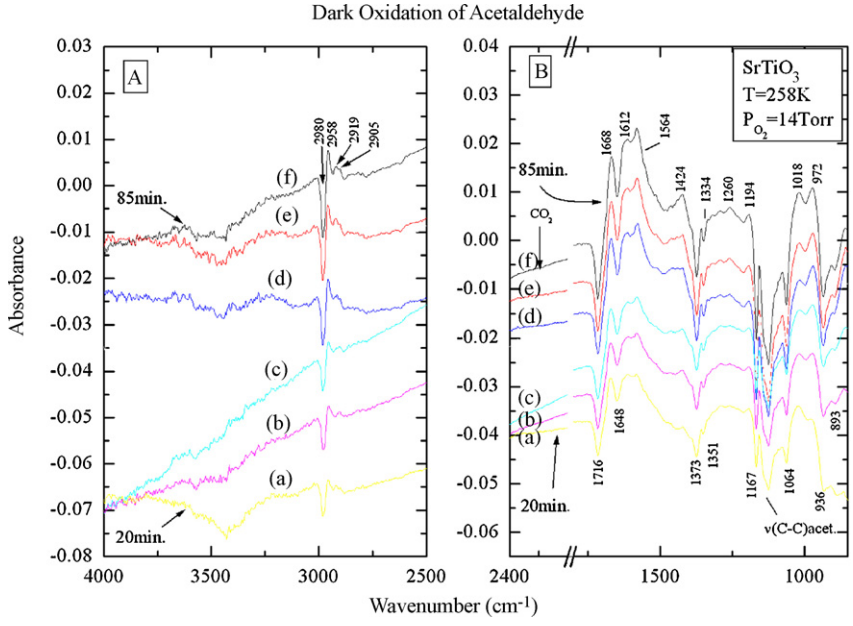

Fig. 5. (A and B) Time dependent subtracted infrared spectra during the reaction of preadsorbed acetaldehyde with oxygen gas in the dark (in absence of UV–vis light) at 258 K. The background used for subtraction is spectrum shown in Fig. 4g.

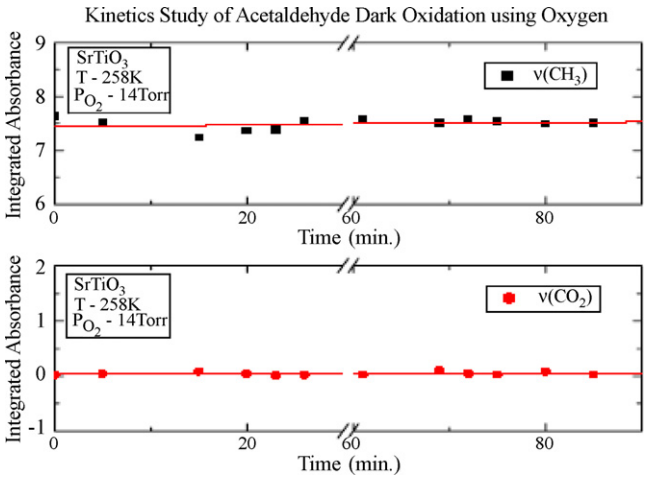

Fig. 6. Time dependent change in integrated absorbance of $\nu(CH_3)$ and $\nu(CO_2)$ during the reaction studied in Fig. 5.

ν(CH) for the entire duration (85 min) of dark oxidation as observed in the plot given in Fig. 6.

The decrease in the ν(CH) (at 2980 cm^{-1}) absorbance may be due to a slight shift in CH stretching mode due to partial oxidation of absorbed aldehyde forming acetate.

3.4. Spectral development during photooxidation reaction

Fig. 7 (reference used for subtraction is the spectrum collected just before photoirradiation) shows that the intensity of CH_3 vibrational modes (at 2964, 2919, and 2862 cm^{-1}) of adsorbed acetaldehyde is significantly attenuated during 149 min of photooxidation. The fact that new CH_3 stretching modes in this spectral region were not observed to be produced during photooxidation indicates that C–H bond oxidation was occurring extensively, and that any intermediate species containing CH_3 bonds were of low surface coverage.

Simultaneously, various carbonyl and carboxyl stretching modes due to aldehyde, carboxylate, and formate developed, as shown in Table 3.

The gradual production of gas phase CO_2 was observed for CH_3CHO photooxidation reaction for a continuous period of 150 min at 273 K as shown in Fig. 7. The CO_2 is the final oxidation product, often referred to as the mineralization product because of the extreme level of oxidation which it represents. It must represent the result of multiple elementary photooxidation steps as molecules as complex as acetaldehyde and crotonaldehyde are destroyed by the production of a sequence of intermediate oxidation products which ultimately reach CO_2. However, no CO formation was observed during photooxidation.

As photooxidation took place over a period of 149 min, the intensity of the H-bonded Ti–OH mode at 3680 cm^{-1} decreased slightly as acetaldehyde/crotonaldehyde molecules were gradually destroyed. This suggests that the photooxidation products containing carbonyl, carboxyl or water are also H-bonded which caused the red-shift of Ti-OH mode by ~200 cm^{-1}.

The spectral region below 2000 cm^{-1} contains a complex overlap of vibrational modes which undergo systematic changes in absorbance as photooxidation takes place. The observation of modes which increase or decrease in absorbance can be observed most conveniently by presenting the difference spectra obtained over the course of the photooxidation experiments, and this has been indicated in Fig. 7. Table 3 summarizes these results and presents a tentative assignment of each mode. Simultaneous growth of bands, attributed to various carbonyl stretching modes due to aldehyde, carboxylate, formate, and carbonate were observed.

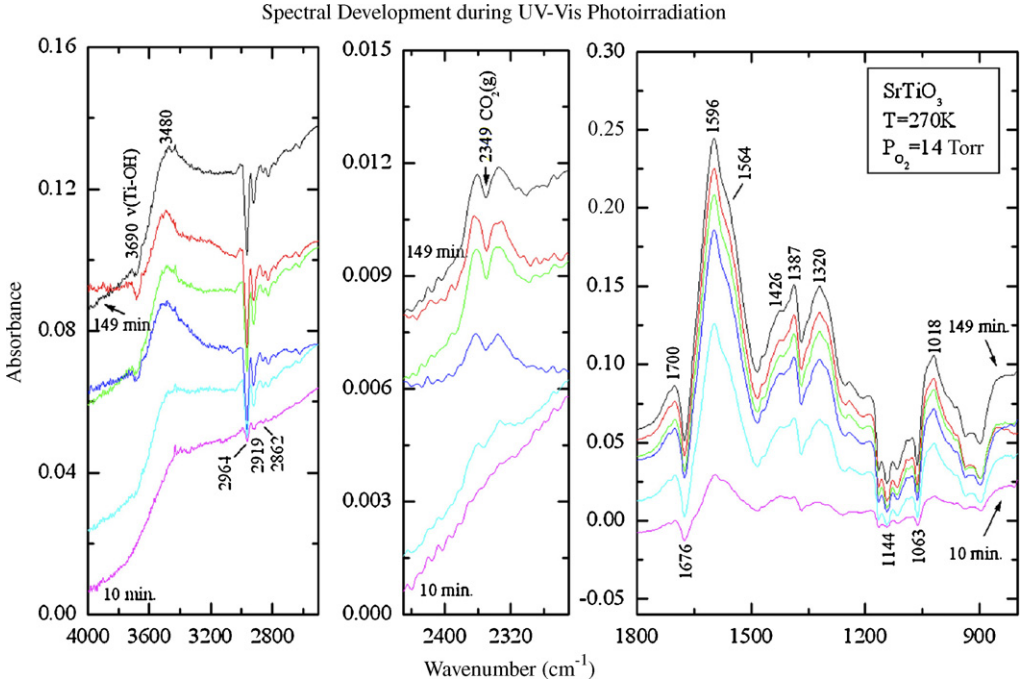

Fig. 7. Infrared spectra of oxidation of preadsorbed acetaldehyde in presence of oxygen during photoirradiation with UV–vis light.

Table 3
Vibrational frequency (cm^{-1}) and assignments of adsorbed species during photooxidation of acetaldehyde over $SrTiO_3$

Frequency (cm^{-1})	Species formed during oxidation	Frequency (cm^{-1})	Spectral features depleted during oxidation
2353	CO_2	1676	Carbonyl $\nu(C{=}O)_{as}$
1700	Carbonyl $\nu(C{=}O)_{as}$	1144	$\nu(C{-}C)$
1596/1564	Carboxyl $\nu(OCO)_{as}$	1063	$\nu(C{-}O)$
1424/1378	Carboxyl $\nu(OCO)_s$	938	$\gamma_r(CH_3)$
3680 decrease	Ti–OH···OCO	2964	$\nu_{as}(CH_3)$
3480 increase		2919	$\nu_s(CH_3)$
		2862	$\nu(CH)$

Adsorption of acetic acid on this catalyst showed bands at 1560 cm^{-1} ($\nu_a OCO$), 1458 cm^{-1} ($\delta_a CH_3$), 1391 cm^{-1} ($\nu_s OCO$), 1340 cm^{-1} ($\delta_a CH_3$), and 1021 cm^{-1} (ρCH_3) (spectrum not shown). The shape and location of these bands are closely similar to the spectra obtained during photooxidation experiments indicating that a large fraction of acetaldehyde formed acetate species including other minor products. These frequencies and assignment of carboxylate species are consistent with studies of acetic acid over different metal oxide surfaces such as CeO_2 [31], TiO_2 [25], Fe_2O_3 [33], and UO_2 [32]. One of the products suspected to have formed during photochemical oxidation was CH_3CH_2OH, however, the key infrared features for ethoxide species for TiO_2 such as ν(C–O) band at 1119 and 1042, and $\omega(CH_2)$ at 1356 cm^{-1} are missing [34].

Fig. 8 gives a summary of the rates of photooxidation as observed from the changes in infrared absorbances obtained for acetaldehyde photooxidation at 270 K. Here the depletion of absorbances for the CH_3 and >C=O modes of acetaldehyde is shown along with kinetics of production of carboxylate and CO_2 gas. The baseline against which these peak absorbances are measured is empirically adjusted to compensate for baseline shifts which have been characterized in other investigations. These baseline shifts correspond to the production and consumption of trapped conduction band electrons as the photochemistry progresses. A more sophisticated kinetic comparison is not warranted by the data. Here the depletion of alkyl groups is not correlated with production of CO_2 and carboxylate species because the "half-life" time constants are different for acetaldehyde and oxidized products. This implies that multiple photooxidation steps are involved in the conversion of acetaldehyde into final oxidation products, but our experiments are not sufficiently sensitive to separate the intermediate surface oxidation steps.

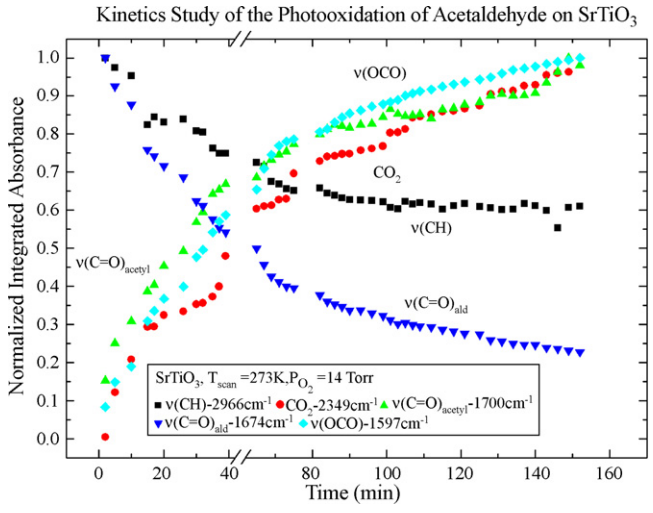

Fig. 8. Kinetic behavior for consumption of acetaldehyde during photooxidation and for production of highly oxidized products.

3.5. Comparison of dark and photooxidation

Acetaldehyde adsorbs reversibly onto the $SrTiO_3$ surface through H-bonding or Lewis acid–base interaction. Upon warming, a fraction of the acetaldehyde ultimately forms crotonaldehyde via aldol condensation and exposure to oxygen. In the dark, the adsorbed acetaldehyde and crotonaldehyde undergo mild oxidation forming carboxylate (crotonate and acetate) and other oxidized species, such as peroxyacetate species. In the presence of UV photoirradiation, the partially oxidized species acetate and peroxyacetate undergo extensive oxidation forming CO_2 and other oxidized species.

3.6. Conclusions

Strontium titanate nanoparticles of diameter ~8 nm and surface area 159 m^2/g were synthesized using aerogel procedure. These nanoparticles were characterized by X-ray diffraction and transmission electron microscopy along with BET surface area measurements. In addition, adsorption of acetaldehyde and its reactivity on aerogel prepared $SrTiO_3$ nanoparticles were investigated by transmission infrared spectroscopy for different temperature domains. This infrared study also focused on the influence of UV light in bonding and decomposition of acetaldehyde. The following conclusions have been obtained. (1) Acetaldehyde adsorbs onto the surface –OH groups at 233 K through H-bonding of carbonyl group [Ti–OH···O=C(H)CH_3]. A fraction of acetaldehyde also adsorbs through Lewis acid sites (Ti^{4+} or Ti^{3+} ion). (2) Upon warming the adsorbed aldehyde undergo self condensation reaction forming 3-butanal, which undergoes dehydration forming 2-butenal surface species with two key modes of vibration ν(C=O) mode at 1667 cm^{-1} and a weak ν(C=C) mode at 1644 cm^{-1}. (3) Photooxidation of adsorbed acetaldehyde at 270 K results in formation of CO_2 (2349 cm^{-1}) as well as other partially oxidized products such as acetate and/or crotonate surface species. (4) No

carbon monoxide formation was observed during photodecomposition.

Acknowledgments

We gratefully acknowledge with thanks the support of this work by NSF, ONR and DOD Multidisciplinary University Research Initiative (MURI) program administered by the Army Research Office.

References

[1] A.L. Linsebigler, G. Lu, J.T. Yates Jr., Chem. Rev. 95 (1995) 735–758.
[2] W. Xu, D. Raftery, J. Phys. Chem. B 105 (2001) 4343–4349.
[3] Li.-Q. Wag, K.F. Ferris, J. Phys. Chem. B 108 (2004) 1646–1652.
[4] A. Fujishima, K. Honda, Nature 37 (1972) 238.
[5] Miggli, S. Darrin, J.L. Falconer, J. Catal. 187 (1999) 230.
[6] F. Gracia, J.P. Holgado, A. Caballero, A.R. Gonzalez-Elipe, J. Phys. Chem. B 108 (2004) 17466.
[7] C.A. Jenkins, D.M. Murphy, C.C. Rowlands, T.A. Egerton, J. Chem. Soc., Perkin Trans. 2 (1997) 2479.
[8] T. Tachikawa, S. Tojo, K. Kawai, M. Endo, M. Fujitsuka, T. Ohno, M. Nishijima, T. Majima, J. Phys. Chem. B 108 (2004) 19299.
[9] T. Ohno, S. Izumi, K. Fujihara, Y. Masaka, M. Matsumura, J. Phys. Chem. B 104 (2000) 6801.
[10] D.A. Panayotov, D.K. Paul, J.T. Yates Jr., J. Phys. Chem. B 107 (2003) 10571.
[11] T.L. Thompson, D.A. Panayotov, J.T. Yates Jr., I. Martyanov, K. Klabunde, J. Phys. Chem. B 108 (2004) 17857.
[12] K.J. Klabunde (Ed.), Nanoscale Materials in Chemistry, John Wiley and Sons, Inc., 2001 (chapter 2).
[13] D. Demydov, Klabunde, J. Kenneth, J. Non-Cryst. Solids 350 (2004) 165.
[14] A.F. Bedilo, K.J. Klabunde, Nanostruct. Mater. 8 (2) (1997) 119.
[15] T.H. Ballinger, J.C.S. Wong, J.T. Yates Jr., Langmuir 8 (1992) 1676.
[16] P. Basu, T.H. Ballinger, J.T. Yates Jr., Rev. Sci. Instrum. 59 (1988) 1321.
[17] S. Peter, H.D. Lutz, Z. Anorg. Allg. Chem. 624 (1998) 1067.
[18] S. Hunsche, A. Grone, G. Greten, S. Kapphan, R. Pankrath, J. Seglins, Phys. Status Solidi (a) 148 (1995) 629.
[19] J. Baltrusaitis, V. Grassian, J. Phys. Chem. B 109 (2005) 12227.
[20] D.K. Paul, C. Marten, J.T. Yates Jr., Langmuir 15 (1999) 4508.
[21] Z. Liu, J. Tabora, R.J. Davis, J. Catal. 149 (1994) 117.
[22] D. Panayotov, J.T. Yates Jr., J. Phys. Chem. B 107 (2003) 10560–10564.
[23] L.-Q. Wang, K.F. Ferris, S. Azad, M.H. Engelhard, C.H.F. Peden, J. Phys. Chem. B 108 (2004) 1646.
[24] R.N. Spitz, J.E. Barton, M.A. Barteau, M.A. Staley, A.W. Sleight, J. Phys. Chem. 90 (1986) 4067.
[25] J. Boaventura, Ph.D. Thesis, University of Delaware, 1989.
[26] A.A. El-Azhary, R.H. Hilal, Spectrochim. Acta 53 (1997) 1365.
[27] J.C. Jesus, F. Zaera, Surf. Sci. 430 (1999) 99.
[28] S. Luo, J.L. Falconer, J. Catal. 185 (1999) 393.
[29] H. Idriss, M.A. Barteau, Catal. Lett. 40 (1996) 147.
[30] H. Idriss, M. Libby, M.A. Barteau, Catal. Lett. 15 (1992) 13.
[31] A. Yee, S. Morrison, H. Idriss, J. Catal. 186 (1999) 279.
[32] H. Madhavaran, H. Idriss, J. Catal. 224 (2004) 358.
[33] M.A. Natal-Santiago, J.M. Hill, J.A. Dumesic, J. Mol. Catal. 199 (1999) 140.
[34] I. Carrizoosa, G. Munuera, J. Catal. 49 (1977) 174.